Unidirectional Thermal Diffusion in Bimetallic Cu@Au Nanoparticles

Shoujie Liu,[†,§] Zhihu Sun,[†,§] Qinghua Liu,[†] Lihui Wu,[†] Yuanyuan Huang,[†] Tao Yao,[†,*] Jing Zhang,[‡] Tiandou Hu,[‡] Mengran Ge,[†] Fengchun Hu,[†] Zhi Xie,[†] Guoqiang Pan,[†] and Shiqiang Wei[†,*]

[†]National Synchrotron Radiation Laboratory, University of Science and Technology of China, Hefei, Anhui 230029, People's Republic of China, and [‡]Beijing Synchrotron Radiation Facility, Institute of High Energy Physics, Chinese Academy of Sciences, Beijing 100049, People's Republic of China. [§]These authors contributed equally to this work.

ABSTRACT Understanding the atomic diffusions at the nanoscale is important for controlling the synthesis and utilization of nanomaterials. Here, using *in situ* X-ray absorption spectroscopy coupled with theoretical calculations, we demonstrate a so far unexplored unidirectional diffusion from the Au shell to the Cu core in thermally alloying Cu@Au core@shell architecture of *ca.* 7.1 nm. The initial diffusion step at 423 K is found to be characterized by the formation of a diffusion layer composed of a Au-dilute substitutional CuAu-like intermetallic compound with short Cu−Au bond length (2.61 Å). The diffusion further happens by the migration of the Au atoms with large disorder into the interior Cu matrix at higher temperatures (453 and 553 K). These results suggest that the structural preference of a CuAu-like compound, along with the nanosized effect, plays a critical role in determining the atomic diffusion dynamics.

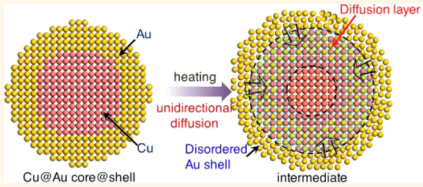

KEYWORDS: unidirectional atomic diffusion · core@shell nanoparticle · *in situ* X-ray absorption spectroscopy · Cu@Au · dilute substitutional intermetallic

The diffusion of atoms is an important phenomenon, which determines the rates and pathways of countless chemical reactions and structural transformations. The atomic diffusion in nanoscale matters has been intensively employed in the design of new nanodevices and nanomaterials.[1,2] For example, the Kirkendall effect, which is based on different diffusion rates of two species, has been used to cave nanomaterials with defined cavities, such as hollow nanoparticles (NPs) and 3D objects with maze-like interiors.[3,4] Moreover, bimetallic NPs with controlled structure, such as core@shell, are attractive materials owing to their novel optical, catalytic, and electronic properties that are different from those of their monometallic counterparts.[5] The atomic diffusion is a fundamental issue for the core@shell NPs in their controlled synthesis, as well as their stabilities in the use of catalytic reactions. Therefore, a detailed understanding of these atomic diffusion processes at the nanoscale is essential to design new bimetallic nanomaterials with optimal structures and properties.

Conventionally, diffusion in solids was studied by experimentally profiling the depth dependence of trace atoms, or by theoretically developing a diffusion model,[6,7] which gave a macroscopic parameter of diffusion constant. To observe the atomic diffusion, *in situ* high-resolution transmission electron microscopy or scanning tunneling microscopy techniques have been employed to follow the atomic motions, but they could only probe the surface atoms.[8−10] Recently, Leitner *et al.* reported a possible opportunity based on the coherent X-ray to reveal the diffusive motion of atoms as a function of their neighborhoods in a Cu−Au alloy single crystal.[11] To date, the mechanistic studies on the atomic diffusion in nanomaterial systems are rarely reported. On the other hand, the diffusion reported usually occurs mutually at finite temperature for two contacted agents with similar forms and structures (Figure 1).[7,12] This bidirectional mode is complex, making it inconvenient to design microstructures and functions of binary materials through the control of the diffusion. Different from the bidirectional model, the unidirectional diffusion means that only diffusion from one species to another matrix is rarely reported experimentally to our knowledge, except for a previous theoretical predication by molecular dynamics simulations.[13] Therefore, if the

* Address correspondence to yaot@ustc.edu.cn, sqwei@ustc.edu.cn.

Received for review December 13, 2013 and accepted January 28, 2014.

Published online January 28, 2014
10.1021/nn4063825

diffusion could be controlled in a unidirectional manner, we would effectively manipulate the diffusion behaviors and reveal some new aspects on the diffusion mechanism.

In this work, using *in situ* X-ray absorption fine structure (XAFS) technique in combination with the theoretical calculations, we present a study on the atomic evolutions during the thermal diffusion in the core@shell NPs. We use Cu@Au architecture of ~7.1 nm as our samples because of the significantly enhanced thermal diffusion effect, as well as of their well-understood binary phase diagram.[1,14] The thorough diffusion of two metal elements allows one to probe this process using temperature-dependent XAFS, which has proven to be effective for following the atomic motions across the thermally induced phase transition in VO_2.[15] The high precision temperature controller enables us to control the temperature variation of ±0.2 °C. As a result, the temperature evolution sequence could be obtained to probe the thermally induced diffusion process. A unidirectional diffusion route from Au→Cu is discovered, in spite of their comparable diffusivities in bulk.

RESULTS AND DISCUSSION

The Cu@Au NPs were synthesized by a sequential reduction that involves the reduction of a second metal onto the preformed cores.[16,17] The resulting Cu NPs have a mean diameter of 5.5 ± 0.4 nm (Figure 2a), which were subsequently coated with a Au shell by adding $HAuCl_4$/oleylamine to the Cu colloid at 90 °C. The Cu@Au NPs have a mean size of 7.1 ± 0.5 nm, as shown in Figure 2b. Considering the precursors' feed ratio and the analysis on the edge jump of the X-ray absorption,[18] we evaluated a ~1:2 stoichiometry of Au/Cu in the sample. A high-resolution TEM (HRTEM) image confirms the successful preparation of the core–shell nanostructure (Figure 2c). The core size and shell thickness are measured to be 5.5 and 0.74 nm, respectively. The lattice fringes corresponding to the face-centered cubic (fcc) (111) planes in the Au shell and Cu core are clearly seen.[19] Furthermore, the high-angle annular dark-field scanning TEM (HAADF-STEM) characterization is performed. The element mapping on a single particle obviously indicates a core–shell structure consisting of Cu as a core and a complete shell of Au (Figure 2c). Some grain boundaries exist in the interior of the Cu core, which do not have a large influence on the diffusion behaviors occurring at the Cu–Au interface.

The UV–vis spectra in Figure 3a collected at different reaction times show that the Au covering on the Cu core blue shifts the surface plasmon resonance absorbance from 563 nm for the Cu seed to 520 nm expected for the Au NPs.[20] Also, the coating of Au on Cu is confirmed by the X-ray diffraction pattern (XRD) in which only the diffraction peaks from fcc Au are observed (Figure 3b). This is probably due to the heavy atom effect of Au, which is consistent with the previous report for the Au coating the Fe_3O_4 core.[21] The above results confirm the well-controlled core@shell nanostructure, providing an ideal model to investigate the thermally induced diffusion process. It is widely accepted that the XRD technique is limited by its identification of the small amount of species in the matrix;[22,23] it is hence not suitable for studying the small evolutions of atomic local structures in the early stage of diffusion. Moreover, the diffraction pattern for Cu@Au NPs clearly shows the shielding effect of the Au shell, implying that it could be hard to detect the

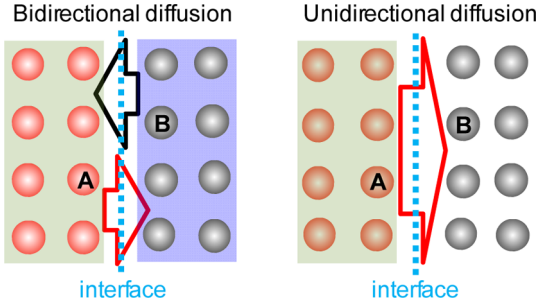

Figure 1. Schematic drawings of two diffusion models: the left panel represents the bidirectional diffusion involving A→B accompanied by B→A. The right panel shows the unidirectional diffusion where only A diffuses into the B matrix.

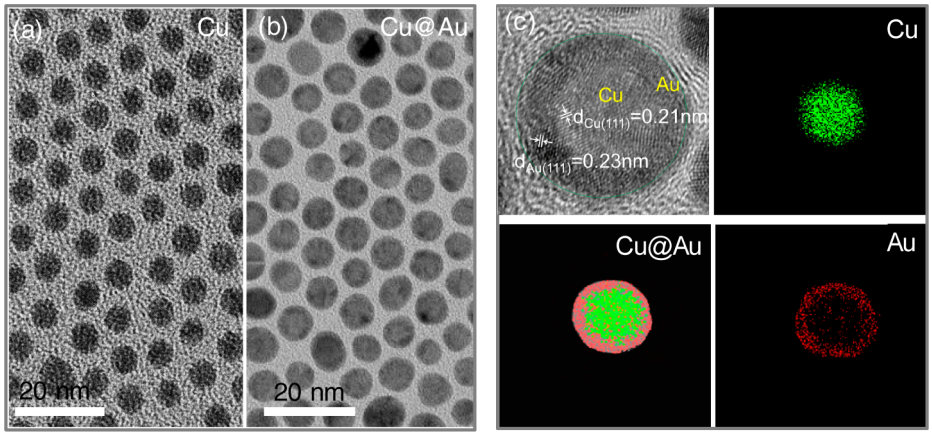

Figure 2. TEM images of (a) initial Cu core and (b) Cu@Au NPs. (c) HRTEM and HAADF-STEM-EDS mapping images of a Cu@Au NP.

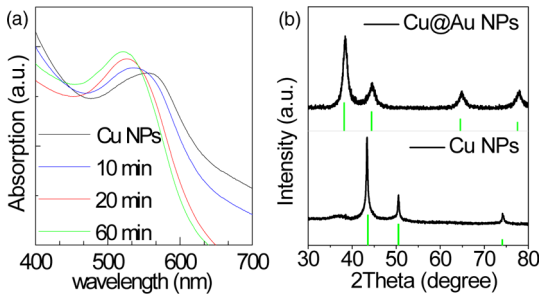

Figure 3. (a) UV−vis spectra collected at different times during the Au coating. (b) Typical XRD pattern of Cu core and Cu@Au NPs.

changes occurring at the interface inside the system. Alternatively, the XAFS has its special advantage in element selectivity and in determining the interatomic distances with high accuracy (~0.01 Å)[24] and is suited to separately probe and compare the atomic evolutions at the interface *in situ* during the diffusion of two species.

Figure 4a,b shows the Au L_3-edge *in situ* XAFS spectra of Cu@Au NPs within the temperature range of 298−533 K. Also, *in situ* XAFS data of the unary ~7 nm Au NPs are shown in Figure 4c for comparison. Evidently, the $k\chi(k)$ oscillation curves for the Cu@Au NP samples below 423 K show the spectral features of fcc Au. When heated to 423 K or higher, slight changes in the k regions of around ~5 $Å^{-1}$ and >10 $Å^{-1}$ can be observed (Figure 4a), which can also be identified in the corresponding FT profiles (Figure 4b). First, the two peaks at 2.39 and 2.85 Å attributed to the nearest Au−Au pair rapidly decrease in intensity with temperature and become rather low and nearly vanish at 453 K and above, indicative of the disappearance of Au fcc-structured features. This temperature-dependent damping of the amplitude looks very similar to the *in situ* XAFS results for unary Au particles (Figure 4c), for which the peaks at higher temperatures are weakened by the thermal disorder effects.[25] Second, it is important to note that when the temperature reaches 423 K, the Cu@Au sample possesses a new coordination peak at around 2.20 Å, whose intensity is further enhanced by increasing the temperature to 453 K and eventually it saturates at 553 K. The emergence of this coordination peak, however, is not observed for unary Au NPs at any temperature. Hence, the 2.20 Å FT peak could only be ascribed to the Au−Cu pair formed at elevated temperature, evidencing thermally induced diffusion in the Cu@Au NPs.

Interestingly, in contrast to the striking changes of Au L_3-edge XAFS results, the $k\chi(k)$ and corresponding FTs for Cu K-edge XAFS spectra exhibit nearly identical features at all temperatures (Figure 4d,e). The gradually decreased intensity of the nearest Cu−Cu peak at 2.20 Å with temperature is consistent with the *in situ* XAFS results for the unary Cu particles of ~7 nm (Figure 4f), except for the appearance of a side lobe at 423 K or

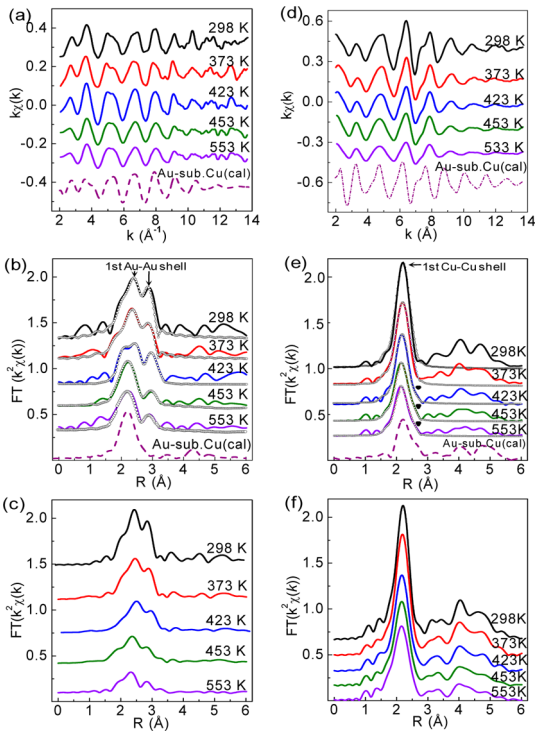

Figure 4. Temperature-dependent *in situ* XAFS spectra. Au L_3-edge EXAFS oscillations [$k\chi(k)$] (a) and their FTs for (b) Cu@Au NPs and (c) 7 nm Au NPs at several temperatures during the heating process. Cu K-edge EXAFS oscillations [$k\chi(k)$] (d) and their FTs for (e) Cu@Au NPs and (f) 7 nm Cu NPs at the corresponding temperatures.

higher (marked by the triangle). However, its intensity is much lower as compared with the notable Au−Cu peak in Au L_3-edge XAFS, suggesting that the crystal lattice of fcc Cu experiences little change in the diffusion. Moreover, it should be noted that the experimental curves at 453 and 553 K fairly match with the calculated EXAFS FTs using the model of Au randomly substituting for Cu sites in Cu sublattice (noted as "Au-sub. Cu") at each edge. This manifests the formation of the substitutional CuAu alloy, which is reasonable because of the similar crystal phases (fcc) and electronic shell closings ($d^{10}s^1$) between Au and Cu.

The above experimental evidence of the unitary change for the Au structure leads us to consider that the thermally induced diffusion in the Cu@Au is in a unidirectional way from Au (shell)→Cu (core). The quantitative structural information was extracted from least-squares curve fittings using the module ARTEMIS of the IFEFFIT code (Table 1).[26,27] At 423 K, the $R_{Au-Cu/Cu-Au}$ is about 2.61 Å in the diffusion layer, close to that (2.65 Å) of the Cu_3Au_1 compound and also to that (2.63 Å) for the $Cu_{1-x}Au_x$ alloy with small proportion of Au (<30%).[28] According to Vegard's law, the $R_{Au-Cu/Cu-Au}$ is larger than 2.70 Å when Au content amounts to 50%, as in the Cu_1Au_1 (tetragonal, R = 2.71 Å) and Cu_1Au_3 (cubic, R = 2.81 Å) compounds.[1,29] Hence, we consider that the diffusion layer composed of the substitutional CuAu-like intermetallic compound is formed in the

TABLE 1. Structural Parameters Extracted from Quantitative EXAFS Curve Fittings from Au L_3-Edge Data[a]

T (K)	bond	R (Å)	N	σ^2 (10^{-3} Å^2)	σ_s^2 (10^{-3} Å^2)	σ_T^2 (10^{-3} Å^2)
298	Au−Au (shell)	2.87 ± 0.02	9.6 ± 0.5	7.6 ± 0.5	1.6 ± 0.4	6.0 ± 0.4
373	Au−Au (shell)	2.87 ± 0.03	9.6 ± 0.6	8.3 ± 1.1	1.6 ± 0.4	6.7 ± 0.4
423	Au−Au (shell)	2.87 ± 0.04	8.9 ± 0.3	13.1 ± 0.8	5.6 ± 0.5	7.5 ± 0.5
	Au−Cu (D-layer)	2.61 ± 0.02	7.3 ± 0.5	10.6 ± 0.6	3.6 ± 0.5	7.0 ± 0.5
	Au−Au (D-layer)	2.73 ± 0.04	1.5 ± 0.5	10.0 ± 0.9	2.5 ± 0.6	7.5 ± 0.6
453	Au−Cu (D-layer)	2.62 ± 0.03	6.4 ± 0.6	14.2 ± 0.6	6.1 ± 0.6	8.1 ± 0.6
	Au−Au (D-layer)	2.74 ± 0.03	2.5 ± 0.4	15.0 ± 0.8	6.5 ± 0.6	8.5 ± 0.6
553	Au−Cu (D-layer)	2.62 ± 0.02	6.4 ± 0.4	15.3 ± 0.7	6.1 ± 0.6	9.2 ± 0.6
	Au−Au (D-layer)	2.74 ± 0.03	2.5 ± 0.4	15.7 ± 0.8	6.5 ± 0.6	9.2 ± 0.6

[a] D-layer denotes the diffusion layer; *N* is the coordination number; σ^2 is the mean square relative displacement, which is the sum of two contributions: the structural disorder (σ_s^2) and the thermal disorder (σ_T^2). The detailed analysis procedures to obtain the σ_s^2 and σ_T^2 are described in Experimental Section.

TABLE 2. Structural Parameters Extracted from Quantitative EXAFS Curve Fittings from Cu K-Edge Data

T (K)	bond	R (Å)	N	σ^2 (10^{-3} Å^2)	σ_s^2 (10^{-3} Å^2)	σ_T^2 (10^{-3} Å^2)
298	Cu−Cu (core)	2.55 ± 0.02	11.4 ± 0.4	8.5 ± 1.0	2.8 ± 0.6	5.7 ± 0.4
373	Cu−Cu (core)	2.55 ± 0.02	11.4 ± 0.5	9.2 ± 1.0	2.8 ± 0.6	6.4 ± 0.4
423	Cu−Cu (core)	2.55 ± 0.03	10.3 ± 0.2	9.9 ± 1.0	2.9 ± 0.5	7.0 ± 0.5
	Cu−Cu (D-layer)	2.55 ± 0.04	7.8 ± 0.3	10.2 ± 0.9	3.2 ± 0.5	7.0 ± 0.5
	Cu−Au (D-layer)	2.61 ± 0.03	2.1 ± 0.4	10.5 ± 0.9	3.0 ± 0.5	7.5 ± 0.6
453	Cu−Cu (D-layer)	2.56 ± 0.02	7.0 ± 0.3	14.3 ± 0.8	6.2 ± 0.6	8.1 ± 0.6
	Cu−Au (D-layer)	2.62 ± 0.02	3.3 ± 0.4	14.3 ± 0.8	6.8 ± 0.6	8.5 ± 0.6
553	Cu−Cu (D-layer)	2.56 ± 0.02	7.0 ± 0.4	15.4 ± 0.8	6.2 ± 0.6	9.2 ± 0.6
	Cu−Au (D-layer)	2.62 ± 0.02	3.3 ± 0.5	16.0 ± 0.8	6.8 ± 0.6	9.2 ± 0.6

initial diffusion stage. In this layer, the Au atoms of a small quantity are dominantly surrounded by Cu because the random configuration with nearest-neighbor pairs of unlike atoms is favored in the Au−Cu system.[11] Moreover, the ratio between coordination number, N_{Au-Cu}/N_{Cu-Au} = 7.3/2.1 ≈ 3.5 at 423 K, also indicates the low Au proportion of about ∼20% in the early diffusion stage, further validating our assumption that the diffusion occurs mainly from Au→Cu. If a substantial interdiffusion involving the migration of some Cu atoms into the Au matrix, or a unidirectional diffusion from Cu to Au had occurred, a new FT peak should arise in Cu K-edge XAFS and the $R_{Au-Cu/Cu-Au}$ should be as large as ∼2.70 Å or even 2.80 Å (Table 2).[1] Moreover, the interdiffusion of Au and Cu would produce the diffusion layer with comparable content of Au and Cu because of the similar diffusion coefficients between Au and Cu. The outward diffusion of Cu might also be possible at low temperature of ≤423 K in the initial diffusion stage, which means that further diffusion of Cu outward would be limited by this layer with high Cu content. However, the gradually enhanced Au−Cu pair, along with the faint Au−Au signals in XAFS data with the increased temperature (Figure 4b), indicates the further diffusion and complete alloying of Au and Cu at high temperature, disproving this hypothesis. Therefore, we consider that the possibility of the diffusion of a small amount of Cu atoms into the Au matrix at low temperature is small, and the unidirectional diffusion of Au→Cu is dominant in the whole thermal diffusion process.

There are three possible diffusion ways, including unidirectional diffusion of Cu→Au, interdiffusion of Au↔Cu, and unidirectional diffusion of Au→Cu. They correspond to the formation of the interlayer containing Au-rich intermetallic compound (noted as "CuAu-I"), intermetallic compound with the same content of Cu and Au ("CuAu-II"), and the Cu-rich one ("CuAu-III"), separately. To find the possible driving force for the unidirectional diffusion, we performed a series of first-principles calculations to examine which intermetallic compound would be more stable, using Vienna ab initio simulation package (VASP). Accordingly, these three distinct interlayer intermetallic compounds were considered in the calculations. The unit cell parameters were 2.80, 2.70, and 2.61 Å for CuAu-I, CuAu-II, and CuAu-III models, respectively, based on the EXAFS results. We calculated the formation energy to determine the relative stability of different configurations, for which the formation energy was calculated as $E_f = E_{tot} - m\mu_{Au} - n\mu_{Cu}$, where the E_{tot} is the total energies of the corresponding models. Here, the μ_{Au} and μ_{Cu} are the atom chemical potentials of Au and Cu, respectively, while *m* and *n* are the numbers of Au and Cu atoms in the calculations. The calculated formation energy for the CuAu-III model is −5.54 eV, smaller than the values of −5.49 and −5.42 eV for the CuAu-II and CuAu-I models, respectively (Figure 5a). The calculations show that the formation of a Au-dilute CuAu-like intermetallic compound is most favored in the diffusion layer. Hence, we consider that the structural stability during the alloying

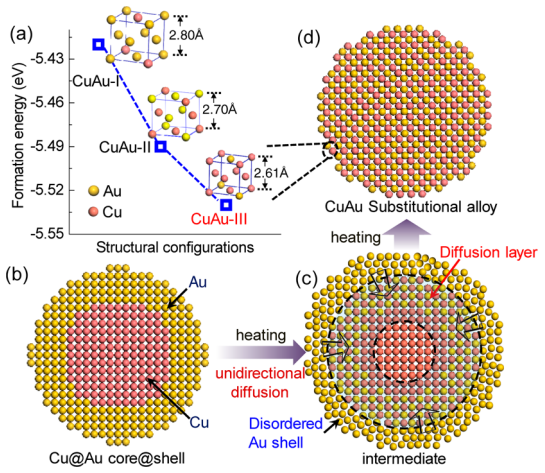

Figure 5. (a) Formation energies for different structural configurations: CuAu-I (Au-rich), CuAu-II (equal quantity), and CuAu-III (Cu-rich) substitutional intermetallic compounds models. (b–d) Schematic of the thermally activated diffusion process for Cu@Au NPs. Upon heating, the shell-disordered Au atoms unidirectionally diffuse into the Cu core, forming a Au-dilute substitutional CuAu-like intermetallic compound (c). With the proceeding diffusion, the diffusion region swells, and a completely substitutional alloy is formed (d).

of Au and Cu plays the major role in driving the unidirectional diffusion. This is indeed similar to the previous theoretical prediction that had indicated the unidirectional diffusion of Cu to Ag core, which was also ascribed to the stable structures of isolated Cu impurities inside different Ag cores.[13] Similar structure-dominated diffusion has been demonstrated in a previous report, where the crystal vacancies at the interface of Au@Ag were found to cause the spontaneous interdiffusion between the two metals.[30]

Based on the above combined analysis of experimental and calculation results, a picture could be drawn regarding the thermal diffusion process, as illustrated in Figure 5b–d schematically. In Cu@Au NPs, the Au shell has a larger proportion of surface atoms that have large surface stress and would be more affected than the Cu core which remains in the fcc phase (Figure 5b). The strong uniaxial pressure that arises from the surface stress in the Au shell would significantly depress the melting temperature for the Au shell. Hence, by increasing temperature, the Au shell has already transformed into a more disordered state relative to the Cu core, which can be reflected by a large increase of static structure disorder (σ_s^2) of 0.0040 ± 0.0004 Å^2 for the Au shell from 298 to 423 K. On the contrary, the Cu–Cu structural disorder factor shows a slight increase of 0.0001 ± 0.0007 Å^2, along with the remaining features of the Cu–Cu peak beyond the nearest neighbor in the Cu XAFS spectra. Meanwhile, the heat treatment will to some extent induce atomic vibrations and lattice expansions, especially in NPs,[31] providing more space for the diffusing Au atoms with extremely high motilities into the Cu core. During the nanoscale alloying, the structural reconstruction occurs,[32] and thereby a diffusion layer composed of compound-like structures with a small amount of Au atoms doped into the Cu sublattice is formed (Figure 4c). The size mismatch between Au and Cu atoms then makes the lattice in this layer strongly distorted, as suggested by the large σ^2 (0.014–0.015 Å^2) of Au–Cu pairs. As the diffusion proceeds, the increased temperature drives continuously the one-way migration of the outside Au atoms into the diffusion layer and interior Cu core. Hence, the diffusion layer volume is always expanding while the pure Cu core volume is shrinking due to the incorporation of Au atoms macroscopically. However, from the microscopic picture, the Cu atoms at the Cu/Au interface would not diffuse actively toward the Au layer (Figure 5d). These results suggest that the thermally-increased structural disorder in the nanostructured Au shell provides a driving force for the diffusion of Au atoms, while the preferred stability of structural preference of the Au-dilute CuAu-like compound determines the unidirectional diffusion behavior.

CONCLUSIONS

In summary, we have performed an *in situ* study on the thermally activated diffusion process in the Cu@Au bimetallic systems. Contrary to the conventional interdiffusion route, our *in situ* measurements evidence a dominant unidirectional diffusion route involving the migration of the Au shell atoms into the Cu core upon heating and forming a diffusion layer composed of substitutional CuAu-like intermetallic compounds. The first-principles calculations confirmed the energetically favored formation of the substitutional CuAu fcc alloy with dilute Au distribution. The presented results will provide more implications for manipulating the diffusion process, for example, by turning the structures or the composites in bimetallic systems.

EXPERIMENTAL SECTION

Synthesis of Cu@Au NPs. First, the Cu core NPs were synthesized using a modification approach for the synthesis of CuO. In a typical synthesis, 1 mmol copper(I) acetate (CH_3CO_2Cu,), 1 mL of oleic acid, and 10 mL of trioctylamine were prepared in a flash. The mixture was heated to 180 °C in a nitrogen atmosphere under magnetic stirring for 1 h and then quickly heated to 270 °C for an hour after it was cooled to 120 °C. Finally, the color of the solution became dark red. Then, the Cu core was sacrificed to replace Au ions to form the core@shell structure. Four milliliters of oleylamine containing 1 mmol $HAuCl_4$ was rapidly injected into the above mixing solution under vigorous stirring, generating a black solution. The solution was reacted at 160 °C for an hour under flowing nitrogen. The obtained core@shell Cu@Au NPs were washed by 100 mL of ethanol and then were segregated three times at 10 000 rpm for 10 min.

Finally, the Cu@Au NPs were kept in a vacuum drying chamber. Then, 100 mg of graphite powder was added into hexane by dissolving 11 mg of dried core@shell Cu@Au NPs and used ultrasonic to mix them homogeneously. The mixture solution was dried in a vacuum drying oven, and the dried sample was pressed into a pellet in a stainless steel holder and used to collect the X-ray absorption data.

Characterizations. Powder XRD data were collected at U7B stations of the National Synchrotron Radiation Laboratory, China. Energy-dispersive X-ray spectroscopy (EDS) analysis and high-resolution transmission electron microscopy (TEM) image were obtained by a JEM-2010 TEM. The samples for TEM were prepared by dropping the reaction solution onto copper TEM grids directly and drying in air. UV−vis spectra were recorded with a Shimadzu SOLID3700 spectrophotometer.

***In Situ* XAFS Measurement.** Temperature-dependent XAFS spectra at the Au L_3 (11919 eV) and Cu K (8979 eV) edges were measured in transmission mode at the U7C and U7B beamlines of the National Synchrotron Radiation Laboratory, 1W1B beamline of Beijing Synchrotron Radiation Facility and BL14W1 beamline of Shanghai Synchrotron Radiation Facility, China. The detailed instrumental information can be found in our previous report.[15] The storage ring of NSRL was working at the energy of 800 MeV with an average electron current of 300 mA. The hard X-ray was monochromatized with Si(111) double crystals. The high precision temperature controller enables us to control the temperature variation of ±0.2 °C. In our *in situ* XAFS experiment, the core@shell sample was first heated to the given temperature (298, 373, 423, 453, and 533 K) and then kept at the measuring temperatures for 20 min during the data acquisition. The XAFS data for the sample at each temperature were collected two times to obtain the high-quality data, and acquisition of an EXAFS spectrum requires 5 min. It was found that the multiple-scan XAFS data can be well-replicated, indicating that the sample can stay in a dynamic equilibrium without further diffusion at each temperature.

XAFS Data Analysis. The EXAFS data analysis and fitting strategy were performed using the IFEFFIT package.[26,27] The quantitative information can be obtained by the least-squares curve fitting in the *R* space with a Fourier transform *k* space range of 2.2−13 $Å^{-1}$, using the module ARTEMIS of programs of IFEFFIT. Effective scattering amplitudes and phase shifts of all the paths for fitting the EXAFS data were calculated by the *ab initio* code FEFF8.0. The structural parameters, such as the coordination number *N*, the interatomic distance *R*, and the Debye−Waller factor σ^2 (discussed below), were allowed to vary during the fitting process.

The σ^2 corresponds to the mean square relative displacement (MSRD) among two atoms and is the sum of two contributions:[33,34]

$$\sigma^2 = \sigma_s^2 + \sigma_T^2 \quad (1)$$

The first term σ_s^2 is temperature independent and associated with the static structural disorder, while the second (dynamical) contribution σ_T^2 is due to thermal vibrations and can be correlated to the vibrational spectrum of the system. The latter could be approximated by the Einstein model:

$$\sigma_T^2 = \frac{\hbar^2}{2k\mu}\frac{1}{T_E}\coth\left[\frac{T_E}{2T}\right] \quad (2)$$

where μ is the reduced mass of the atom pair, T is the temperature, k is Boltzmann's constant, and $\hbar$ is Plank's constant. $T_E = (\hbar/k)\omega_E$ is the Einstein temperature, and ω_E is the corresponding Einstein frequency. For our Cu@Au nanostructure, however, the static disorder itself changes with increasing temperature. Therefore, the routinely used method of separating the static disorder from the thermal disorder could not be applied directly. Instead, we obtained the thermal disorders σ_T^2 of the Cu−Cu and Au−Au bonds in the elemental Au and Cu nanoparticles using the above-mentioned method, and the results are roughly approximated as those for the Cu@Au nanostructure. For this purpose, we performed a fitting of the experimental data of elemental Au and Cu NPs with the Einstein model and obtained the values of T_E (125 and 185 K) and σ_s^2 (0.0012 and 0.0020 $Å^2$) for elemental Au and Cu NPs (see Supporting Information). Consequently, the values of the thermal disorders can be calculated as for Au−Au bonds and Cu−Cu bonds at corresponding temperatures. These values of thermal disorder can be approximated to the σ_T^2 values for the Cu@Au samples at each temperature. Regarding the diffusion layer, since the reference AuCu compounds could hardly be synthesized or characterized by *in situ* XAFS, we have to approximately represent the σ_T^2 of Au−Au and Cu−Cu bonds in elemental NPs as the σ_T^2 of Cu−Au and Au−Cu bonds in the diffusion layer which have the same scattering atoms. Hence, the structural disorders, σ_s^2, in the Cu@Au samples can be deduced by subtracting these thermal disorder contributions according to eq 1.

Conflict of Interest: The authors declare no competing financial interest.

Acknowledgment. This work is financially supported by the National Natural Science Foundation of China (11135008, U1232132, 11079032, and 11175184), the National Basic Research Program of China (2012CB825800), the Foundation for Innovative Research Groups of the National Natural Science Foundation of China (11321503), and by the Fundamental Research Funds for the Central Universities (WK2310000026). The authors would like to thank NSRL, SSRF, and BSRF for the beam time.

Supporting Information Available: Temperature dependence of the Debye−Waller factors, σ^2, for the 7 nm Au and Cu NPs, with their respective Einstein models. This material is available free of charge *via* the Internet at http://pubs.acs.org.

REFERENCES AND NOTES

1. Ferrando, R.; Jellinek, J.; Johnston, R. L. Nanoalloys: From Theory to Applications of Alloy Clusters and Nanoparticles. *Chem. Rev.* **2008**, *108*, 845–910.
2. Graetzel, M.; Janssen, R. A. J.; Mitzi, D. B.; Sargent, E. H. Materials Interface Engineering for Solution-Processed Photovoltaics. *Nature* **2012**, *488*, 304–312.
3. Yin, Y.; Alivisatos, A. P. Colloidal Nanocrystal Synthesis and the Organic−Inorganic Interface. *Nature* **2005**, *437*, 664–670.
4. Gonzalez, E.; Arbiol, J.; Puntes, V. F. Carving at the Nanoscale: Sequential Galvanic Exchange and Kirkendall Growth at Room Temperature. *Science* **2011**, *334*, 1377–1380.
5. Chaudhuri, R. G.; Paria, S. Core/Shell Nanoparticles: Classes, Properties, Synthesis Mechanisms, Characterization, and Applications. *Chem. Rev.* **2012**, *112*, 2373–2433.
6. Dominguez, G.; Wilkins, G.; Thiemens, M. H. The Soret Effect and Isotopic Fractionation in High-Temperature Silicate Melts. *Nature* **2011**, *473*, 70–73.
7. Zhang, B.; Griesche, A.; Meyer, A. Diffusion in Al−Cu Melts Studied by Time-Resolved X-ray Radiography. *Phys. Rev. Lett.* **2010**, *104*, 035902.
8. Chen, K. C.; Wu, W. W.; Liao, C. N.; Chen, L. J.; Tu, K. N. Observation of Atomic Diffusion at Twin-Modified Grain Boundaries in Copper. *Science* **2008**, *321*, 1066–1069.
9. Grant, M. L.; Swartzentruber, B. S.; Bartelt, N. C.; Hannon, J. B. Diffusion Kinetics in the Pd/Cu(001) Surface Alloy. *Phys. Rev. Lett.* **2001**, *86*, 4588–4591.
10. Anderson, M. L.; D'Amato, M. J.; Feibelman, P. J.; Swartzentruber, B. S. Vacancy-Mediated and Exchange Diffusion in a Pb/Cu(111) Surface Alloy: Concurrent Diffusion on Two Length Scales. *Phys. Rev. Lett.* **2003**, *90*, 126102.
11. Leitner, M.; Sepiol, B.; Stadler, L. M.; Pfau, B.; Vogl, G. Atomic Diffusion Studied with Coherent X-rays. *Nat. Mater.* **2009**, *8*, 717–720.
12. Van der Ven, A.; Ceder, G. First Principles Calculation of the Interdiffusion Coefficient in Binary Alloys. *Phys. Rev. Lett.* **2005**, *94*, 045901.
13. Baletto, F.; Mottet, C.; Ferrando, R. Growth of Three-Shell Onionlike Bimetallic Nanoparticles. *Phys. Rev. Lett.* **2003**, *90*, 135504.
14. Sra, A. K.; Schaak, R. E. Synthesis of Atomically Ordered AuCu and $AuCu_3$ Nanocrystals from Bimetallic Nanoparticle Precursors. *J. Am. Chem. Soc.* **2004**, *126*, 6667–6672.

15. Yao, T.; Zhang, X. D.; Sun, Z. H.; Liu, S. J.; Huang, Y. Y.; Xie, Y.; Wu, C. Z.; Yuan, X.; Zhang, W. Q.; Wu, Z. Y.; *et al.* Understanding the Nature of the Kinetic Process in a VO_2 Metal-Insulator Transition. *Phys. Rev. Lett.* **2010**, *105*, 226405.
16. Yu, H.; Gibbons, P. C.; Kelton, K. F.; Buhro, W. E. Heterogeneous Seeded Growth: A Potentially General Synthesis of Monodisperse Metallic Nanoparticles. *J. Am. Chem. Soc.* **2001**, *123*, 9198–9199.
17. Habas, S. E.; Lee, H.; Radmilovic, V.; Somorjai, G. A.; Yang, P. Shaping Binary Metal Nanocrystals through Epitaxial Seeded Growth. *Nat. Mater.* **2007**, *6*, 692–697.
18. Li, Y. Y.; Liu, S. J.; Yao, T.; Sun, Z. H.; Jiang, Z.; Huang, Y. Y.; Cheng, H.; Huang, Y. Y.; Jiang, Y.; Xie, Z.; *et al.* Controllable Synthesis of Gold Nanoparticles with Ultrasmall Size and High Monodispersity *via* Continuous Supplement of Precursor. *Dalton Trans.* **2012**, *41*, 11725–11730.
19. Chen, W.; Yu, R.; Li, L.; Wang, A.; Peng, Q.; Li, Y. A Seed-Based Diffusion Route to Monodisperse Intermetallic CuAu Nanocrystals. *Angew. Chem., Int. Ed.* **2010**, *49*, 2917–2921.
20. Xia, Y.; Xiong, Y.; Lim, B.; Skrabalak, S. E. Shape-Controlled Synthesis of Metal Nanocrystals: Simple Chemistry Meets Complex Physics? *Angew. Chem., Int. Ed.* **2009**, *48*, 60–103.
21. Xu, Z. C.; Hou, Y. L.; Sun, S. H. Magnetic Core/Shell Fe_3O_4/Au and Fe_3O_4/Au/Ag Nanoparticles with Tunable Plasmonic Properties. *J. Am. Chem. Soc.* **2007**, *129*, 8698–8699.
22. Billinge, S. J. L.; Levin, I. The Problem with Determining Atomic Structure at the Nanoscale. *Science* **2007**, *316*, 561–565.
23. Wei, H.; Yao, T.; Pan, Z. Y.; Mai, C.; Sun, Z. H.; Wu, Z. Y.; Hu, F. C.; Jiang, Y.; Yan, W. S. Role of Co Clusters in Wurtzite Co: ZnO Dilute Magnetic Semiconductor Thin Films. *J. Appl. Phys.* **2009**, *105*, 043903.
24. Yano, J.; Kern, J.; Sauer, K.; Latimer, M. J.; Pushkar, Y.; Biesiadka, J.; Loll, B.; Saenger, W.; Messinger, J.; Zouni, A.; *et al.* Where Water Is Oxidized to Dioxygen: Structure of the Photosynthetic Mn_4Ca Cluster. *Science* **2006**, *314*, 821–825.
25. Frenkel, A. I.; Vasic, R.; Dukesz, B.; Li, D.; Chen, M. W.; Zhang, L.; Fujita, T. Thermal Properties of Nanoporous Gold. *Phys. Rev. B* **2012**, *85*, 195419.
26. Ravel, B.; Newville, M. Athena, Artemis, Hephaestus: Data Analysis for X-ray Absorption Spectroscopy Using IFEFFIT. *J. Synchrotron Radiat.* **2005**, *12*, 537–541.
27. Knecht, M. R.; Weir, M. G.; Frenkel, A. I.; Crooks, R. M. Structural Rearrangement of Bimetallic Alloy PdAu Nanoparticles within Dendrimer Templates To Yield Core/Shell Configurations. *Chem. Mater.* **2008**, *20*, 1019–1028.
28. Frenkel, A. I.; Machavariani, V. S.; Rubshtein, A.; Rosenberg, Y.; Voronel, A.; Stern, E. A. Local Structure of Disordered Au-Cu and Au-Ag Alloys. *Phys. Rev. B* **2000**, *62*, 9364–9371.
29. Hennig, J.; Mari, D.; Schaller, R. Order−Disorder Phase Transition and Stress-Induced Diffusion in Au-Cu. *Phys. Rev. B* **2009**, *79*, 144116.
30. Shibata, T.; Bunker, B. A.; Zhang, Z. Y.; Meisel, D.; Vardeman, C. F.; Gezelter, J. D. Size-Dependent Spontaneous Alloying of Au−Ag Nanoparticles. *J. Am. Chem. Soc.* **2002**, *124*, 11989–11996.
31. Fornasini, P.; Beccara, S. A.; Dalba, G.; Grisenti, R.; Sanson, A.; Vaccari, M.; Rocca, F. Extended X-ray-Absorption Fine-Structure Measurements of Copper: Local Dynamics, Anharmonicity, and Thermal Expansion. *Phys. Rev. B* **2004**, *70*, 174301.
32. Yin, J.; Shan, S.; Yang, L.; Mott, D.; Malis, O.; Petkov, V.; Cai, F.; Ng, M. S.; Luo, J.; Chen, B. H.; *et al.* Gold−Copper Nanoparticles: Nanostructural Evolution and Bifunctional Catalytic Sites. *Chem. Mater.* **2012**, *24*, 4662–4674.
33. Balerna, A.; Mobilio, S. Dynamic Properties and Debye Temperatures of Bulk Au and Au Clusters Studied Using Extended X-ray-Absorption Fine-Structure Spectroscopy. *Phys. Rev. B* **1986**, *34*, 2293–2298.
34. Greegor, R. B.; Lytle, F. W. Extended X-ray Absorption Fine-Structure Determination of Thermal Disorder in Cu-Comparison of Theory and Experiment. *Phys. Rev. B* **1979**, *20*, 4902–4907.